ChemBioChem

Research Article
doi.org/10.1002/cbic.202300270

Chemistry Europe
European Chemical Societies Publishing

www.chembiochem.org

Modulating Secondary Structure Motifs Through Photo-Labile Peptide Staples

Ilze Lāce,[a] Sophia Bazzi,[b] Jon Uranga,[b] Anastasiya Schirmacher,[a] Ulf Diederichsen+,[a] Ricardo A. Mata,[b] and Nadja A. Simeth*[a, c]

Peptide-protein interactions (PPIs) are facilitated by the well-defined three-dimensional structure of bioactive peptides, interesting compounds for the development of new therapeutic agents. Their secondary structure and thus their propensity to engage in PPIs can be influenced by the introduction of peptide staples on the side chains. In particular, light-controlled staples based on azobenzene photoswitches and their structural influence on helical peptides have been studied extensively. In contrast, photolabile staples bearing photocages as a structural key motif, have mainly been used to block supramolecular interactions. Their influence on the secondary structure of the target peptide is under-investigated. Thus, in this study we use a combination of spectroscopic techniques and *in silico* simulations to systematically study a series of helical peptides with varying length of the photo-labile staple to obtain a detailed insight into the structure-property relationship in such photoresponsive biomolecules.

Introduction

Bioactive peptides have attracted increasing attention as they are promising platforms for the development of novel therapeutic compounds.[1] They are a group of biopolymers typically consisting of up to 50 amino acid (AA) residues[2] and combine the high target specificity of proteins with the bioavailability of classical drugs.[3] Compared to proteins, they show reduced allergenic effects,[4] and their intrinsic biocompatibility results in a reduced potential of toxic effects in the body compared to traditional small molecule pharmaceuticals.[5]

They interact with their biological targets in protein-peptide interactions (PPIs) through their well-defined three-dimensional structure. Among these, different types of secondary structures have been identified as recognition motifs. For instance, α-helices, β-sheets, and their mimetics can form targeted interactions with protein surfaces.[6–9]

Suitable peptides can be further modified to enhance target affinity, inhibitory properties, metabolic stability, and cellular uptake. For instance, staples can be introduced on the side chains of the AA residues to reduce conformational flexibility and thus constrict the bioactive peptide in its active 3D-structure.[10–12] Frequently used staples are based on disulfide bridges (Cys side chains),[13] amide bonds (Lys, Asp, Glu side chains),[14,15,77] or hydrocarbon bridges (unnatural amino acids (UAAs)).[16–18] (Figure 1A).

While the introduction of peptide staples facilitates a permanent enhancement of the peptide's biological activity, classical staples cannot be regulated dynamically and thus, the modified peptide will always remain in its active form. However, it has been shown to be advantageous for biological probes[19–21] or in medicinal chemistry to modulate biological activity on demand by application of a stimulus.[22–24]

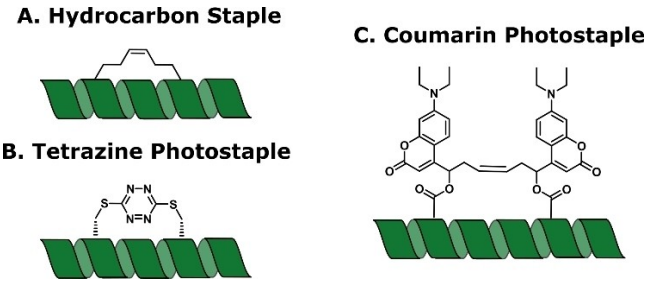

Figure 1. A. Permanently stapled peptide. **B**. Tetrazine staple utilizing cysteine side chains. **C**. Coumarin-based photostapled peptide presented in this work.

[a] *I. Lāce, A. Schirmacher, Prof. Dr. U. Diederichsen,+ Prof. Dr. N. A. Simeth*
Institute for Organic and Biomolecular Chemistry
Department of Chemistry
University of Göttingen
Tammannstr. 2, 37077 Göttingen (Germany)
E-mail: nadja.simeth@uni-goettingen.de

[b] *S. Bazzi, J. Uranga, Prof. Dr. R. A. Mata*
Institute for Physical Chemistry
Department of Chemistry
University of Göttingen
Tammannstr. 6, 37077 Göttingen (Germany)

[c] *Prof. Dr. N. A. Simeth*
Cluster of Excellence "Multiscale Bioimaging: from Molecular Machines to Networks of Excitable Cells" (MBExC)
Universitätsmedizin Göttingen
Robert-Koch-Str. 40, 37075 Göttingen (Germany)

[+] *Deceased on November 11, 2021*

Supporting information for this article is available on the WWW under https://doi.org/10.1002/cbic.202300270

This article is part of the Special Collection ChemBioTalents2022. Please see our homepage for more articles in the collection.

In this context, light has served as a superior stimulus as it can be applied with superb spatiotemporal precision.[25,26] Moreover, the usage of photons as reagents is beneficial as they can be applied externally and are traceless reagents by nature.[27] In this manner, photoresponsive small bioactive molecules,[26,28–32] nucleotides,[33–37] UAAs,[38–41] and peptides[41–47] have been developed.

A frequently used light-responsive structural motif are photocages, *i.e.* photolabile protecting groups, that can be attached to a biologically active structure to inactivate it.[48–50] They are particularly appealing due to their typically high OFF-ON difference in bioactivity as a result of the large structural change upon irradiation and uncaging.[51] They have been previously used, for example, as photoactivated prodrugs,[52,53] photoresponsive block copolymers,[54] and light-induced hydrogels.[55]

Also, light-responsive peptide staples to inhibit PPIs have been reported.[56,57] For instance, a tetrazine photocage (Figure 1B) was employed to first covalently staple and secondly, photochemically unstaple a short peptide to create a library of peptides that could be used for protein target screening due to tetrazines ability to react with target proteins.[57,58] In contrast, azobenzene photoswitches are frequently used to reversibly control PPIs by stabilizing or destabilizing the peptide's 3D structure, depending on the configuration of the photoswitch.[24,56,59,60] However, due to the larger structural change, the biological effect of photochemical uncaging is often higher than the one observed after photoswitching.[61]

Also, the effect of photoswitching on the secondary structure of the functionalized peptide was studied extensively,[61–67] while photocages are typically used to impair functional groups or PPI sites.[68,69] A structural insight into the influence of photocaged bioactive peptides and photocaged staples on the 3D structure of defined secondary structures is under investigated.

To close this gap, we developed photolabile peptide staples based on coumarin-photocages (Figure 1C). In our design, two Lys side chains are decorated with alkene-extended coumarins that can be incorporated into a model peptide by solid phase peptide synthesis (SPPS) and cyclized by Grubbs metathesis to form the final staple. By varying both the linker length of the staple and the position of the photocaged Lys bearing the staple, we systematically analyze the effect that the attached staples and the size of the created macrocycle have on the secondary structure and the supramolecular interactions of the model peptides using a combination of spectroscopic techniques and molecular dynamic (MD) simulations. All-atom MD simulations provide details on the temporal evolution of secondary structures of unmodified and stapled peptides.

We envision that our study will provide new insights into the design of light-responsive peptides taking into account both the influence on supramolecular interactions and the impairment of the peptide's 3D-structure by photocages leading to the dynamic control of photocontrolled PPIs.

Nadja A. Simeth perused her doctorate studies with Burkhard König at the University of Regensburg as a fellow of the Studienstiftung des Deutschen Volkes and graduated in 2018 summa cum laude. She afterwards joined the group of Ben L. Feringa at the University of Groningen as a postdoc supported by a Feodor-Lynen Fellowship of the Humboldt Foundation. In autumn 2021, she was appointed as an assistant professor at the University of Göttingen. She is interested in the design of stimuli-responsive bioorganic molecules, light-sensitive probes and labels, as well as chromoselectively addressable supramolecular and biohybrid systems.

Results and Discussion

Synthesis. The UAA bearing the alkene-extended coumarin photocage was synthesized in five steps from 7-diethylamino-4-methylcoumarin (**1**) and Fmoc-Lys-OH (Scheme 1A). In brief, coumarin **1** was oxidized in two steps using DMF-DMA and $NaIO_4$ to result in compound **3** following reported procedures (quant. yield).[70] Next, the alkene handle was introduced either with allyl tributylstannane for the shorter linker (n = 2) or in a Grignard reaction employing a longer linker (n = 4, Scheme 1). The so-obtained alcohols **4a** and **4b** were then reacted with 4-nitrophenyl chloroformate (**5**) and attached to Fmoc-Lys-OH to introduce a carbamate moiety between the photocage core structure and the AA, which is known to enhance the light-mediated uncaging efficiency.[71,78]

Next, we employed automated microwave-assisted SPPS to synthesize our model peptides **8**–**13o** using UAA **7a**. The target-sequences are displayed in Figure 2. We chose to incorporate the UAAs into the K3 peptide as it is a known coiled-coil peptide that consists of three KIAALKE heptad repeats. Furthermore, through a mix of electrostatic and hydro-

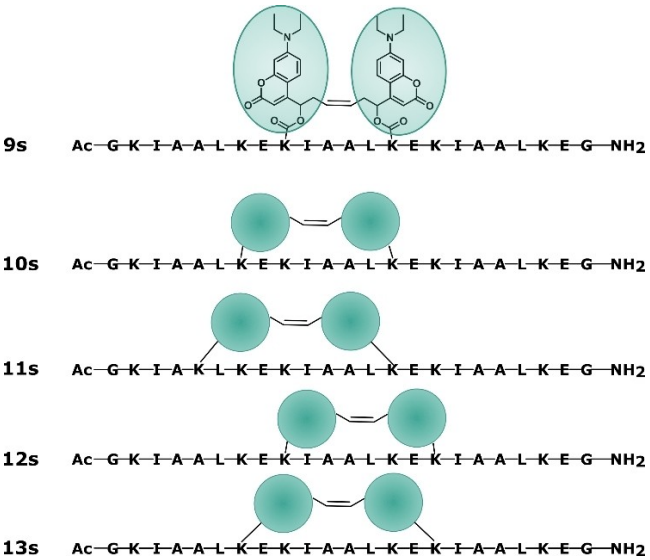

Figure 2. The sequences of the synthesized peptides as well as the positions of the stapled UAAs.

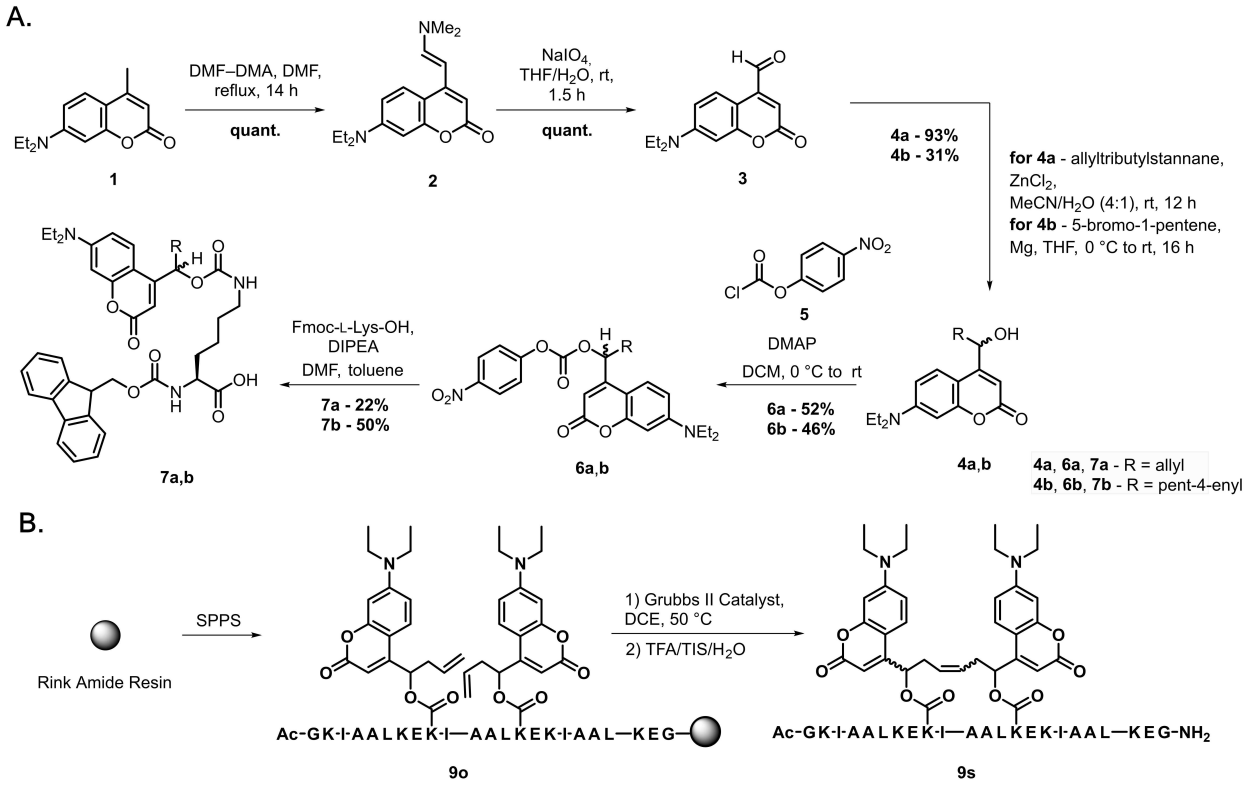

Scheme 1. Synthesis of photocaged UAA **7a**, **7b**. **B**. Synthesis of photo-labile stapled peptides by SPPS and metathesis reaction on resin.

phobic interactions it can form heterodimers with the complementary E3 peptide (consisting of three EIAALEK heptad repeats), which also leads to an increase in the α-helicity of these peptides.[72]

After the peptides were assembled, the photocleavable staple was formed by performing a Grubbs metathesis reaction on resin, generating **9**–**13 s** (Figure 2). Then, the peptides were cleaved from the resin with TFA:TIS:H_2O (95 : 2.5 : 2.5) and purified by reversed phase HPLC. Peptides **9**–**13** could be successfully obtained in both their open (o) and stapled (s) form. However, we found that the metathesis between the two coumarins could not be achieved for over more than 10 amino acid distance. Thus, the longer pent-4-enyl linkage **7b** was developed (Scheme 1B) to also introduce staples in these derivatives. Using the longer linkers, though, could reduce the potential impact by stapling and thus, the influence on the secondary structure of the helical peptides.

To obtain insight into the stability at physiological conditions, we incubated the obtained both open and stapled peptides 9–13 in PBS buffer (pH 7.0, 8 mM Na_2HPO_4, and 2 mM KH_2PO_4). Analysis by UPLC showed that the peptides remained stable over 72 h (for details, see SI, section 8).

Photophysical and Photochemical Characterization. The photoactive UAAs and peptides were in the next step analyzed by UV-Vis spectroscopy. All compounds showed the lowest transition maximum at around 385 nm, which is typically observed for this type of coumarin photocages.[71] The incorporation of the UAAs into the target peptides or the metathesis reaction showed, as expected, hardly any influence on the electronic properties of the coumarin core. Additional absorption bands below 300 nm are ascribed to the electronic transitions of the AAs or the assembled peptide. Also, here, the influence of staple-formation can be omitted.

Next, the light-induced uncaging process of the compounds was followed by *in operando* UV-Vis spectroscopy using a 405 nm LED (for details, see SI, section 6). The spectra of an UAA building block are displayed exemplarily in Figure 3, the

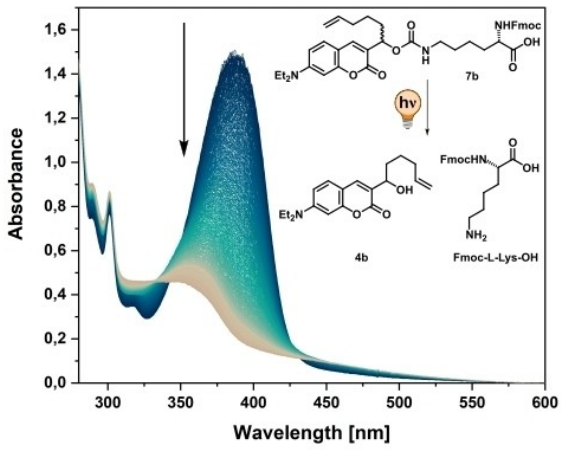

Figure 3. *In operando* UV-Vis absorption spectroscopy of **7b** under irradiation with 405 nm LED light (200 μM, $CHCl_3$, 20 °C, 1 s intervals).

ones of the photo-responsive peptides in the SI. All compounds show that the absorption band around 385 nm decreases upon irradiation, while the deprotected Lys or peptides are formed. The success of the photochemical uncaging reaction was additionally confirmed by ESI-MS analysis. Analysing the efficiency of the uncaging process, we found a photochemical uncaging quantum yield of *ca.* 4% for compound **7a** and was approximated for the peptides to 1–2% (for details, see SI, section 6), which agree with reported values.[78]

DLS and CD Spectroscopy. Next, we studied the influence of the photo-labile staples on the supramolecular interactions of the peptides and on their secondary structure. It is known that **K3** peptides tend to form homodimers and oligomers in solution.[73]

Thus, we analysed our samples using dynamic light scattering (DLS, details see SI, section 5) before and after irradiation to assess the particle sizes. Indeed, we found that the **K3** reference peptide showed particle sizes of 1151 d.nm, which can be ascribed to the formation of oligomers once the peptides were dissolved in buffer. The particles seemed stable in size over a period of 24 h in solution. Analysing the modified peptides exhibiting UAAs, we found that in the case of both the modified peptide in the open form **9o** and the stapled **9s** the particles were smaller in size (398 and 91 d. nm, respectively) than the ones found for **K3**. After irradiation with 405 nm light and accompanied uncaging, the sample showed the formation of larger particles over time (**9o** – 604 d. nm, **9s** – 492 d. nm) and stabilized after *ca.* 24 h. These results indicate, that photo-labile staples in position K9 and K14 can indeed be used to impair the supramolecular interactions between **K3** peptides. Peptides **10o**, **10s**, **11o**, **12o** and **12s** also showed a small increase in particle size after irradiation. However, **13s** and **11s**, with the longest staple, showed a decrease in particle size 24 h after irradiation at 405 nm from 777 d. nm to 412 d. nm for peptide **13s**, and a decrease from 418 d. nm to 354 d. nm for peptide **11s**. This trend was even more pronounced for peptide **13o** (873 d. nm to 412 d. nm).

Unexpectedly, the peptides after uncaging showed a smaller particle size than the unmodified K3 peptide even when the samples were incubated for 24 h to facilitate aggregation. It might be possible that the structural distortion of the photocaged peptides cannot be fully recovered after uncaging (*cf.* CD analysis) or the remaining cleaved coumarin moieties could interfere with the supramolecular assembly process to some extent.

To obtain further insight into the structural modifications imposed by introduction of the UAAs and the uncaging process on the secondary structure of the peptides, we analysed our target compounds by CD spectroscopy and compared the measurements to those of the **K3** reference peptide. We found that both the unstapled peptides (**9o**, **10o**, **11o**, **12o**, **13o**), the stapled ones (**9s**, **10s**, **11s**, **12s**, **13s**) and the unmodified **K3** exhibited negative bands at 222 and 208 nm, which are characteristic for alpha helices. However, peptide K3 exhibits a relatively much more intense negative band at 208 nm than at 222 nm. This is indicative of the fact that without aggregation with its complementary coiled coil counterpart, the helical structure of peptide K3 is distorted.[72,74,75] Therefore, it is important to look at not only the intensity of the CD bands but also their intensity relative to each other, which ideally would be approaching 1.[74] Based on the measured CD spectra, the helical content (hc) was calculated by comparing the measured CD spectra (Figure 4) with a database of spectra with known structures and to assess the effect the UAA has on the secondary structure of the peptide (Table 1, for details see SI, section 4). The staple spanning the shortest distance (**9s**) shows decreased a hc of 9.2%, which increases after irradiation at 405 nm to 18.4%, while the reference **K3** shows a hc of 15.2%. Interestingly, in the open form (**9o**) the extent of helicity is comparable to the hc of the unmodified peptide both before and after irradiation. This points to the fact that the introduction of the UAA does not influence the secondary structure of the parent peptide without stapling. The staples incorporated over longer distances in **10s** and **11s** show in the stapled form a lower hc of 11.3% and 12.4%, respectively, compared to the unmodified peptide. In contrast, the open forms **10o** and **11o** show a reduction in helicity of 8.9% and 11.5% indicating that the photo-labile staple is stabilizing the secondary structure. Furthermore, the helicity is not recovered for **10o** and **11o** after irradiation and as a trend decreases. Interestingly, the staples of peptides **12s** and **13s** show a stabilization of the helical structure (18.7% and 16.2%) which is even stronger in the open forms **12o** and **13o** (22.6% and 24.2%).

For a better comparison with the molecular dynamics (MD) simulations (*vide infra*), we calculated the relative hc comparing the hc of the modified peptides **9**–**13o** and **9**–**13s** with the parent **K3** peptide. A similar trend is observed when comparing experimental and calculated values. The largest deviation is observed in **13s**, which exhibits the largest macrocyclic staple. The relative hc also shows that in peptide **9o** the introduction of the UAAs before stapling hardly affected the helicity. In contrast, stapling into **9s** significantly lowered it indicating a disruption of the structure. Irradiation of both molecules resulted in values comparable to the unmodified **K3**, with the relative hc in **9s** (irrad) being a bit higher than expected. Other derivates, like **10**, **12**, an **13o**, did not show a similar recovery.

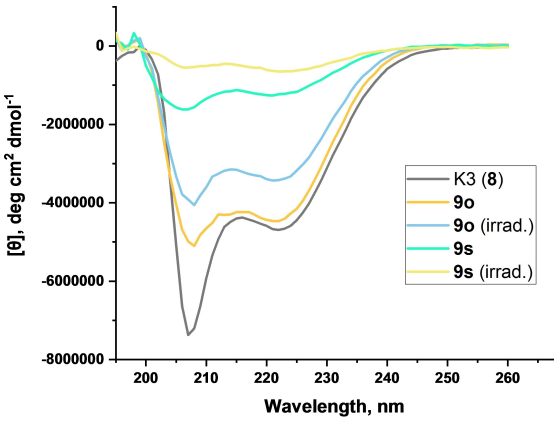

Figure 4. The CD spectra of unmodified K3 peptide (**8**) and unmetathised peptides **9o** and stapled peptide **9s** before and after irradiation at 405 nm in PBS buffer (pH 7.0), 200 μM.

Table 1. The helical content (hc) of peptides **9**–**13** based on their CD spectra calculated using the BeStSel method,[79] their relative hc with respect to the parent **K3** peptide, and their computed relative hc averaged over all production MD frames for each residue.

peptide	helical content (hc)	relative hc [(hc/hc(K3)][a]	computed relative hc [chc/chc(K3)][b]
K3	15.2	1.00	1.00
9o	15.6	1.03	–
9o (irrad)	15.7	1.03	–
9s	9.2	0.61	0.78
9s (irrad)	18.4	1.21	–
10o	8.9	0.59	–
10o (irrad)	7.0	0.46	–
10s	11.3	0.74	0.69
10s (irrad)	9.5	0.63	
11o	11.5	0.76	–
11o (irrad)	10.6	0.70	–
11s	12.4	0.82	0.75
11s (irrad)	10.5	0.69	–
12o	22.6	1.49	–
12o (irrad)	6.2	0.41	–
12s	18.7	1.23	1.11
12s (irrad)	17.5	1.51	–
13o	24.2	1.59	–
13o (irrad)	9.5	0.63	–
13s	16.2	1.07	0.79
13s (irrad)	14.3	0.94	–

[a] The helical content of the peptide derived from its CD spectra over that of the **K3** peptide. [b] Computed average helical propensities of stapled peptides over all frames and residues, relative to **K3**.

On the other hand, the relative hc in **13s** was close to the one of K3 both before and after irradiation, which indicates that its structure and thus, likely its activity are not significantly affected by the addition or removal of the staple. This makes the staples applied in **9** the most promising ones of this study due to their light-induced, reversible impact on the helical structure and their potential to impact the peptide's function.

MD Simulations. Next, we built an *in silico* model of our peptides to evaluate their secondary structures with and without stapling. For this purpose, the FF19SB forcefield was used,[81] adding extra forcefield terms for the linker molecules and specific bonds according to the protocol described in the Supplementary Information. The systems under study were **K3**, **9s**, **10s**, **11s**, **12s**, and **13s**.

All-atom MD simulations were conducted for the above-mentioned systems for a total production time of 400 ns (see Supplementary Information, section 7, for detailed MD simulation protocols). To determine the secondary structure propensities of the peptides, the secondary structure of each protein residue was evaluated using the cpptraj program following the DSSP method by Kabsch and Sander.[76] The results of this analysis are presented in Figure 5, along with the corresponding average backbone structure, for the disordered (None), extended beta ('Ext'), 3–10 helix ('3-10'), α-helix ('Alpha'), 3–14 helix ('3-14') pi ('Pi'), turn ('Turn'), and bend ('Bend') structures, which represent the predominant secondary structures identified by DSSP in the simulations. In order to allow for a fair comparison between theory and experimental measurements, we also present in Table 1 relative helical content values. The latter is defined as the helical content of the molecule measured relative to **K3**. In the case of simulation, one makes use of the DSSP values for each frame and again takes **K3** as the reference.

We now take a closer look at the simulation results. Not surprisingly, all peptides show a high degree of disorder at the terminal residues, but different structural patterns arise along the chain in strong dependence on the modification enacted. The original **K3** peptide shows along the full simulation time an almost perfect alpha helix structure. On the other end of the spectrum, both experiment and simulations show the lowest helical content for the stapled peptides that involve connection of coumarin to lysine 14 (**9s**, **10s**,**11s**). The main contributor to the loss of helicity in **9s** is the expansion of disorder at the terminal residues 14 to 22, and next the residues 13 and 14 that adopt mainly 'Bend' and 'Turn' structures. In case of **10s**, residues 13, 14, 5, 6, and 7 mainly display a 'Turn' structure. On the contrary, the stapled peptides that involve lysine 16 show the largest helix propensity, as shown in Table 1. A net structuring effect for this modification is observed (*cf.* Figure 5).

Conclusions

In summary, we synthesized a coumarin modified UAA with an alkene linkage that can be used to form peptide staples via a Grubb's metathesis reaction. The UAAs with varying linker lengths were then incorporated into a series of **K3** model peptides that have the UAAs at different positions. The ten peptides were obtained via microwave assisted SPPS and characterized regarding their photophysical photochemical characteristics. We found that incorporation of the coumarin core did not significantly affect its lowest electronic transition maximum. Also, irradiation with UV or violet light resulted in photochemical bond cleavage and accompanied liberation of the photocaged lysine in both the coumarin UAAs and the peptide conjugate.

Next, we used DLS analysis of the peptide library to assess the influence of the staple on the aggregation propensity of the K3 derivatives compared to the parent peptides that are known to form oligomers. Comparing samples before irradiation and 24 h after uncaging showed that peptides **9o**, **9s**, **10o**, **10s**, **11o**, **12o**, and **12s** seemed to recover the ability to aggregate, while the same trend was not observed for peptides **11s**, **13o**, and **13s**.

The analysis of the helical content (hc) calculated from the CD spectra showed that the different length staples as well as position affect the peptide secondary structure differently. While peptides **9s**, **10s**, and **11s** were distorted by the staple, the helicity in peptides **12s** and **13s** was stabilized. Most interestingly, in peptide **9o** the introduction of the UAAs before

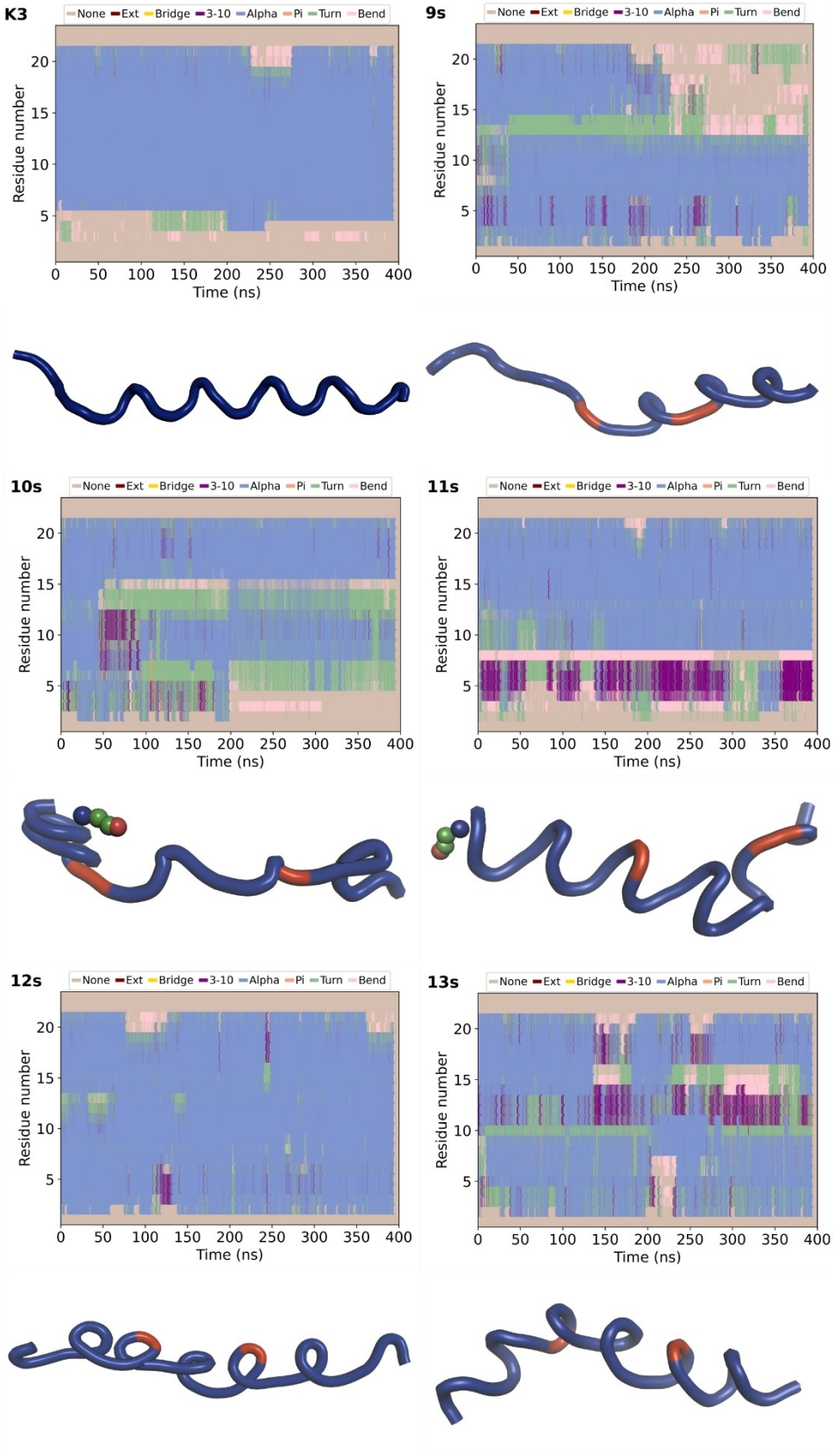

Figure 5. Temporal evolution of secondary structures of the K3 peptide and corresponding modifications, following the DSSP method. The average backbone structures over a 400 ns time span are also presented. For some residues, the disorder was so significant that parts of the peptide chain are displayed as individual spheres.

stapling hardly affected the relative hc, while stapling into **9 s** significantly lowered it. Irradiation of both molecules resulted in values comparable to the unmodified **K3** making the staples applied in **9** the most promising ones of this study. More in detail information about the secondary structures induced by stapling has been provided by MD simulations. The latter demonstrated that the stapled peptides linked to lysine 14 (**9 s**, **10 s**, and **11 s**) exhibit lower helical propensity when compared to the peptides with a connection site at lysine 16 (**12 s**, **13 s**).

In summary, the position and distance of the staples in **9** seem most suitable to reversibly affect the structure, as shown by CD and MD analysis, and supramolecular interactions, indicated by CD and DLS measurements, of K3 peptides. These findings show the potential for this protocol to achieve post-translational modifications with well-defined impact on the secondary structure of peptides.

Experimental Section

Circular Dichroism (CD) Spectroscopy. CD spectroscopic measurements were carried out on a J-1500 CD spectrometer from Jasco (Tokyo, Japan) connected to a F250 recirculation cooler from Julabo (Seelbach, Germany) under continuous flushing with nitrogen. Samples were analysed in a Quartz SUPRASIL QS cuvette with 0.4 cm pathlength from Hellma Analytics (Mühlheim, Germany). Individual spectra were recorded at 20 °C in a wavelength range of 185–265 nm with a bandwidth of 1 nm, response time of 1.0 s, data pitch of 1 nm, and scanning speed of 100 nm/min in "continuous mode". Data was accumulated over 5 measurements.

For better comparability of peptides with different numbers of chromophores (amide bonds) measured, the CD signal was converted to mean residue ellipticity [θ] in deg cm^2 $dmol^{-1}$ by the following formula (1):

$$[\theta] = \frac{\theta_{obs} \cdot MRW}{10 \cdot d \cdot c} \quad (1)$$

where θ_{obs} is the observed ellipticity (deg), MRW is the mean residue molar weight (g mol^{-1}) calculated from the molar weight of the peptide divided by the number of amide bonds, d is the pathlength (cm) and c is the concentration in (g mL^{-1}).

Helical content was calculated using the BeStSel method[79]

Dynamic Light Scattering (DLS). DLS measurements were performed using a Zetasizer Nano S by Malvern Panalytical (Kassel, Germany) with a 633 nm Laser at a probing angle of 173°. All data were acquired using the provided software. Each sample was measured at 25 °C using either disposable semi-micro or macro cuvettes from Brand GmbH (Wertheim, Germany). In case of semimicro cuvettes, single vesicle populations were measured using 100 μL of the sample with 400 μL of buffer. For mixed populations, 500 μL of the sample was used. Using macro cuvettes, 900 μL buffer was added for single vesicle populations. Mixed populations were measured using 1000 μL of the sample. All measurements were performed as triplicates, while individual measurements were obtained with multiple runs between 12–18 times as determined by the software for optimal data quality. The collected data were processed by calculating the weighted arithmetic mean value of each measurement. The hydrodynamic radius (d_h) and PdI (Polydispersity index) were obtained using the instruments software.

UV-Vis Spectroscopy. A nanodrop ND-2000c spectrometer from Thermo Fischer Scientific (Waltham, USA) or a Specord 600 spectrometer with a Quartz SUPRASIL QS cuvette of 0.4 cm path length was used for UV/Vis related measurements. The uncaging was followed while irradiating the cuvette in the spectrometer with a 405 nm LED.

Organic Synthesis

7-(Diethylamino)-4-formylcoumarin (3)

To a solution of 7-(diethylamino)-4-methyl-2H-chromen-2-one **(1)** (5.0 g, 21.6 mmol, 1.00 eq) in DMF (50 mL) was added DMF-DMA (5.75 mL, 43.3 mmol, 2.00 eq). The mixture was heated to reflux and stirred for 16 h.

An aqueous solution of sat. $NaHCO_3$ and DCM were added, the organic layer was separated, and the aqueous layer was extracted with DCM. The combined organic layers were washed with sat. aq. NaCl solution and dried over $MgSO_4$, evaporated under reduced pressure to give crude (E)-7-(diethylamino)-4-(2-(dimethylamino)vinyl)-2H-chromen-2-one **(2)** as a dark orange solid.

This crude compound was then dissolved in THF:H_2O (1 : 1, 90 mL), and $NaIO_4$ was added (13.85 g, 65 mmol, 3.00 eq). The mixture was stirred for 3 h at room temperature, filtered, and the residue washed with EtOAc. THF was evaporated, and sat. $NaHCO_3$ was added. The aqueous layer was extracted with DCM, dried over anhydrous $MgSO_4$ and evaporated under reduced pressure to give crude 7-(diethylamino)-2-oxo-2Hchromene-4-carbaldehyde **(3)** (5.20 g, 21.2 mmol, 98 %) as a dark red oily solid.

TLC: Rf = 0.28 (DCM)

^{1}H-NMR (400 MHz, CDCl3): δ (ppm) = 10.0 (s, 1 H, 11-CHO), 8.28 (d, 3JHH = 9.2 Hz, 1 H, 10-CH), 6.61 (dd, 3JHH = 9.2 Hz, 4JHH = 2.6 Hz, 1 H, 9-CH), 6.50 (d, 4JHH = 2.6 Hz, 1 H, 7-CH), 6.43 (s, 1 H, 1-CH), 3.41 (q, 3JHH = 7.2 Hz, 4 H, 15, 16-CH2), 1.21 (t, 3JHH = 7.1 Hz, 6 H, 17, 18-CH3).

^{13}C-NMR (75 MHz, $CDCl_3$): δ (ppm) = 192.4 (11-CHO), 161.8 (5-C), 157.3 (2-C), 151.0 (8-C), 143.8 (7-C), 128.8 (4-C), 117.2 (1-C), 109.5 (6-C), 103.6 (10-C), 97.5 (3-C), 44.7 (15, 16-CH2), 12.40 (17, 18-CH2).

ESI-MS m/z : 246.1 $[M+H]^+$, 268.1 $[M+Na]^+$.

HR-MS (ESI): calc. for $C_{14}H_{16}NO_3$, ($[M+H]^+$): 246.1127, found: 246.1126; calc. for $C_{14}H_{15}NNaO_3$, ($[M+Na]^+$): 268.0946, found: 246.0944.

7-(Diethylamino)-4-(1-hydroxybut-3-en-1-yl)-coumarin (4 a)

To a solution of 7-(Diethylamino)-4-formylcoumarin **(3)** (1.14 g, 4.64 mmol, 1.00 eq) in MeCN/H_2O (4 : 1, 20 mL) $ZnCl_2$ (1.01 g, 7.40 mmol, 1.60 eq) and allyltributylstannane (2.30 mL, 2.46 g, 7.42 mmol, 1.60 eq) were added and the reaction mixture was stirred for 12 h. MeCN was removed under reduced pressure and H_2O (20 mL) was added. The aqueous suspension was extracted with DCM (3x20 mL). The combined organic phases were washed with brine (10 mL), dried over $MgSO_4$, and adsorbed onto silica (2 g). Purification by column chromatography (hexane/EtOAc 5 : 1 to hexane/EtOAc 3 : 1) gave the product **4 a** (1.23 g, 4.30 mmol, 93 %) as a brown viscous oil.

TLC: Rf = 0.43 (hexane/EtOAc 1 : 1).

^{1}H-NMR (300 MHz, $CDCl_3$): δ (ppm) = 7.37 (d, 3JHH = 9.1 Hz, 1 H), 6.57 (dd, 3JHH = 9.1 Hz, 4JHH = 2.6 Hz, 1 H), 6.48 (d, 4JHH = 2.6 Hz, 1 H), 6.24 (t, 4JHH = 1.3 Hz, 1 H), 5.95-5.80 (m, 1 H), 5.24-5.15 (m, 2 H), 5.01 (dd, 3JHH = 7.89 Hz, 3JHH = 3.7 Hz), 3.39 (q, J = 7.1 Hz, 4 H), 2.71-2.38 (m, 2 H), 1.19 (t, J = 7.1 Hz, 6 H).

^{13}C-NMR (75 MHz, $CDCl_3$): δ (ppm) = 162.4, 157.3, 156.3, 150.2, 133.2, 124.8, 119.1, 108.5, 106.1, 105.4, 98.0, 68.8, 44.7, 12.5.

ESI-MS m/z: 288.2 $[M+H]^+$, 310.2 $[M+Na]^+$, 575.3 $[2M+H]^+$.

HR-MS (ESI): calc. for $C_{17}H_{22}NO_3$, ($[M+H]^+$): 288.1594, found: 288.1594; calc. for $C_{17}H_{21}NNaO_3$, ([M + Na] +): 310.1414, found: 310.1420.

1-(7-Diethylaminocoumarin-4-yl)but-3-en-1-yl (4-nitrophenyl) carbonate (6 a)

7-(Diethylamino)-4-(1-hydroxybut-3-en-1-yl)-coumarin (1.08 g, 3.76 mmol, 1.00 eq) and 4-nitrophenyl chloroformate (**5**) (1.14 g, 5.64 mmol, 1.50 eq) were suspended in DCM (25 mL), cooled with an ice bath, and DIPEA (0.65 mL, 3.76 mmol, 1.00 eq) was added yielding a clear solution. The solution was stirred for 12 h, allowing it to come to room temperature gradually. The newly formed precipitate was dissolved by addition of DIPEA (0.65 mL, 4.0 mmol, 1.0 eq) and the solution was stirred for 1 h. The reaction mixture was directly adsorbed on silica and the crude product was purified by column chromatography (gradient DCM to DCM/acetone 10 : 1). The product **6 a** (0.544 g, 1.20 mmol, 32 %) was obtained as a yellow solid.

TCL: Rf = 0.16 (DCM)

^{1}H-NMR (500 MHz, $CDCl_3$): δ (ppm) = 8.30 (dt, 3JHH = 9.2 Hz, 4JHH = 2.2 Hz, 2 H), 7.42 (d, 3JHH = 9.1 Hz, 1 H), 7.38 (dt, 3JHH = 9.2 Hz, 5JHH = 2.2 Hz, 2 H), 6.60 (dd, 3JHH = 9.1 Hz, 4JHH = 2.6 Hz, 1 H), 6.51 (d, 4JHH = 2.6 Hz, 1 H), 6.17 (s, 1 H), 5.95 (dd, 3JHH = 7.6 Hz, 3JHH = 4.8 Hz, 1 H), 5.88-5.78 (m, 1 H), 5.24–5.17 (m, 2 H), 3.40 (q, 3JHH = 7.1 Hz, 4 H), 2.80–2.67 (m, 2 H), 1.19 (t, 3JHH = 7.1 Hz, 6 H).

^{13}C-NMR (125 MHz, $CDCl_3$): δ (ppm) = 161.8, 156.6, 155.2, 152.4, 151.7, 150.7, 145.5, 131.6, 125.3, 124.6, 121.7, 119.8, 108.9, 105.6, 105.4, 98.1, 75.6, 44.9, 39.0, 12.4.

ESI-MS m/z: 453.2 $[M+H]^+$, 475.2 $[M+Na]^+$.

HR-MS (ESI): calc. for $C_{24}H_{25}N_2O_7$, ($[M+H]^+$): 453.1656, found: 453.1655; calc. for $C_{24}H_{24}N_2NaO_7$, ($[M+Na]^+$): 475.1476, found: 475.1477.

Fmoc-L–Lys(DEACMallyl)-OH (7 a)

Compound **6 a** (0.54 g, 1.24 mmol, 1.00 eq) suspended in DMF/DCM 1 : 1 (20 mL) was combined with Fmoc–L–Lys–OH (0.46 g, 1.24 mmol, 1.00 eq) suspended in toluene/DCM 3 : 2 (30 mL) and cooled in an ice bath. DIPEA (216 μL, 1.24 mmol, 1.00 eq) was added and the reaction mixture was stirred for 12 h allowing it to slowly come to room temperature. Further DIPEA (50 μL, 0.29 mmol, 0.23 eq) was added and the reaction mixture was stirred at rt for 1 h. The solvents were removed under reduced pressure. The residue was dissolved in DCM (50 mL), adsorbed to silica (3 g), and purified by column chromatography (DCM/MeOH/AcOH, 95 : 5 : 0.1). The product **7 a** (178 mg, 1.70 mmol, 22 %) was obtained as a yellow oily solid.

TLC: Rf = 0.29 (DCM/MeOH/AcOH 95 : 5 : 0.1).

^{1}H-NMR (400 MHz, $CDCl_3$): δ (ppm) = 7.72 (d, 3JHH = 7.5 Hz, 2 H), 7.62–7.52 (m, 2 H), 7.41–7.32 (m, 3 H, 7.31–7.24 (t, 3JHH = 7.5 Hz, 2 H), 6.64–6.52 (m, 1 H), 6.52–6.47 (m, 1 H), 6.10 (s, 1 H), 5.95–5.87 (m, 1 H), 5.79–5.72 (m, 1 H), 5.14–5.03 (m, 2 H), 4.44–4.29 (m, 3 H), 4.21–4.14 (m, 1 H), 3.38 (q, 3JHH = 7.0 Hz, 4 H), 3.30–2.96 (m, 2 H), 2.70–2.40 (m, 2 H), 1.96–1.71 (m, 2 H), 1.64–1.27 (m, 4 H), 1.16 (t, 3JHH = 7.2 Hz, 6 H).

^{13}C-NMR (100 MHz, $CDCl_3$): δ (ppm) = 173.7, 163.9, 156.4, 156.2, 155.9, 155.3, 150.6, 143.8, 141.3, 132.4, 127.7, 127.1, 125.2, 124.8, 119.9, 118.5, 109.2, 106.1, 104.0, 98.2, 70.4, 67.0, 53.6, 47.1, 44.9, 40.4, 39.0, 32.0, 28.9, 21.6, 12.6.

ESI-MS m/z: 682.3 $[M+H]^+$, 704.3 $[M+Na]^+$.

HR-MS (ESI): calc. for $C_{39}H_{43}N_3O_8$, ($[M+H]^+$): 682.3050, found: 682.3116; calc. for $C_{39}H_{43}N_3NaO_8$, ($[M+Na]^+$): 704.2948, found: 704.2933.

7-(diethylamino)-4-(1-hydroxyhex-5-en-1-yl)-2H-chromen-2-one (4 b)

Mg shavings (1.68 g, 68.9 mmol, 2.0 eq.) were added to a dried Schlenk flask in argon atmosphere and allowed to stir. Dry THF (60 mL) was added and the reaction mixture was cooled down to 0 °C. 5-bromo-1-pentene (8.2 mL, 69.2 mmol, 2.0 eq.) was added slowly. The reaction mixture was stirred for 1 h and allowed to come up to room temperature slowly. A solution of **1** (8.45 g, 34.5 mmol, 1.0 eq.) in dry THF (40 mL) was added to the reaction mixture and it was stirred for 3 h. The reaction was quenched with sat. aq. NH_4Cl solution and extracted 3 times with diethyl ether, dried over anhydrous $MgSO_4$, filtered and the combined organic phases were evaporated under reduced pressure. The crude product was dissolved in a minimum amount of DCM and purified by automated column chromatography (0–40 % EtOAc in n-Hexane) to yield the product **4 b** (3.60 g, 11.4 mmol, 33 %) as a brown viscous oil.

TLC: R_f = 0.48 (hexane/EtOAc 1 : 1).

^{1}H-NMR (300 MHz, $CDCl_3$): δ (ppm) = 7.45 (d, $^3J_{HH}$ = 9.1 Hz, 1 H), 6.75 (dd, $^3J_{HH}$ = 9.1 Hz, $^4J_{HH}$ = 2.6 Hz, 1 H), 6.54 (d, $^4J_{HH}$ = 2.6 Hz, 1 H), 6.23 (t, $^4J_{HH}$ = 1.3 Hz, 1 H), 5.93-5.62 (m, 4 H), 5.01–4.88 (m, 2 H), 4.57 (dd, $^3J_{HH}$ = 7.89 Hz, $^3J_{HH}$ = 3.7 Hz), 3.40 (q, J = 7.1Hz, 4 H), 3.39–3.25 (m, 2 H), 1.17 (t, J = 7.1 Hz, 6 H).ESI-MS *m/z*: 316.2 $[M+H]^+$, 338.2 $[M+Na]^+$.]$^+$.

HR-MS (ESI): calc. for $C_{19}H_{25}NO_3$, ($[M+H]^+$): 316.1834, found: 316.1907; calc. for $C_{19}H_{25}NNaO_3$, ($[M+Na]^+$): 338.1731, found: 338.1727.

1-(7-(diethylamino)-2-oxo-2H-chromen-4-yl)hex-5-en-1-yl (4-nitrophenyl) carbonate (6 b)

Compound **4 b** (3.60 g, 11.4 mmol, 1.0 eq) and 4-nitrophenyl chloroformate (3.45 g, 17.1 mmol, 1.5 eq) were suspended in DCM (75 mL), cooled with an ice bath, and DIPEA (2.0 mL, 11.4 mmol, 1.0 eq) was added yielding a clear solution. After 30 min DMAP (2.09 g, 17.1 mmol, 1.5 eq.) was added. The solution was stirred for 12 h, allowing it to come to room temperature gradually. The newly formed precipitate was dissolved by addition of DIPEA (2.0 mL, 11.4 mmol, 1.0 eq) and the solution was stirred for 1 h. The reaction mixture was directly adsorbed on silica and the crude product was purified by column chromatography (gradient DCM to DCM/acetone 10 : 1). The product **6 b** (2.5364 g, 5.3 mmol, 31 %) was obtained as a brown oily solid.

TCL: R_f = 0.17 (DCM)

^{1}H-NMR (300 MHz, $CDCl_3$): δ (ppm) = 8.27 (dt, $^3J_{HH}$ = 9.2 Hz, $^4J_{HH}$ = 2.2 Hz, 2 H), 8.13 (d, $^3J_{HH}$ = 9.1 Hz, 1 H), 7.38 (dt, $^3J_{HH}$ = 9.2 Hz, $^5J_{HH}$ =

2.2 Hz, 2 H), 6.62 (dd, $^{3}J_{HH}$ = 9.1 Hz, $^{4}J_{HH}$ = 2.6 Hz, 1 H), 6.52 (d, $^{4}J_{HH}$ = 2.6 Hz, 1 H), 6.14 (s, 1 H), 5.87 (dd, $^{3}J_{HH}$ = 7.6 Hz, $^{3}J_{HH}$ = 4.8 Hz, 1 H), 5.69–5.56 (m, 1 H), 5.08–4.83 (m, 4 H), 3.40 (q, $^{3}J_{HH}$ = 7.1 Hz, 4 H), 2.86–2.77 (m, 2 H), 1.16 (t, $^{3}J_{HH}$ = 7.1 Hz, 6 H).

^{13}C-NMR (75 MHz, $CDCl_3$): δ (ppm) 162.0, 126.2, 124.5, 115.7, 109.1, 97.6, 77.5, 77.0, 76.6, 60.7, 44.8, 31.0, 21.1, 14.2, 12.4.

ESI-MS *m/z*: 481.2 $[M+H]^+$.

Fmoc-l-Lys(DEACM^{pentyl})-OH (7 b)

Compound **6 b** (2.54 g, 5.3 mmol, 1.0 eq) suspended in DMF/DCM 1 : 1 (60 mL) was combined with Fmoc–L–Lys–OH (1.94 g, 5.3 mmol, 1.0 eq) suspended in toluene/DCM 3 : 2 (100 mL) and cooled in an ice bath. DIPEA (919 μL, 5.3 mmol, 1.0 eq) was added and the reaction mixture was stirred for 12 h allowing it to slowly come to room temperature. Further DIPEA (919 μL, 5.3 mmol, 1.0 eq) was added and the reaction mixture was stirred at rt for 1 h. The solvents were removed under reduced pressure. The residue was dissolved in DCM (50 mL), adsorbed to silica (10 g), and purified by column chromatography (DCM/MeOH/AcOH, 95 : 5 : 0.1). The product **7 b** (1.88 g, 2.65 mmol, 50 %) was obtained as a yellow oily solid.

TLC: R_f = 0.35 (DCM/MeOH/AcOH 95 : 5 : 0.1).

^{1}H-NMR (300 MHz, $CDCl_3$): δ (ppm) = 7.76 (d, $^{3}J_{HH}$ = 7.5 Hz, 2 H), 7.64–7.59 (m, 2 H), 7.44–7.35 (m, 3 H), 7.35–7.29 (t, $^{3}J_{HH}$ = 7.5 Hz, 2 H), 6.59–6.53 (m, 1 H), 6.53–6.47 (m, 1 H), 6.12 (s, 1 H), 5.94–5.82 (m, 1 H), 5.82–5.69 (m, 1 H), 5.06-4.94 (m, 2 H), 4.55–4.29 (m, 3 H), 4.27–4.17 (m, 1 H), 3.42 (q, $^{3}J_{HH}$ = 7.0 Hz, 4 H), 3.33–3.08 (m, 2 H), 2.02–1.75 (m, 2 H), 2.07 (m, 2 H), 1.67–1.32 (m, 4 H), 1.26 (t, $^{3}J_{HH}$ = 7.2 Hz, 6 H).ESI-MS *m/z*: 708.3 $[M-H]^-$, 732.3 $[M+Na]^+$.

HR-MS (ESI): calc. for $C_{41}H_{47}N_3O_8$, ($[M-H]^-$): 708.3363, found: 708.3290; calc. for $C_{41}H_{47}N_3NaO_8$, ($[M+Na]^+$): 732.3363, found: 732.3258.

Solid Phase Peptide Synthesis (SPPS). Peptides were synthesized on a on a Rink amide resin (0.44 mmol/g). The following commercially available L-amino acid (aa) building blocks were used in automated microwave assisted SPPS. Building blocks synthesized for this work were coupled by manual microwave assisted SPPS (see below) after transfer of the resin from the synthesizer reaction vessel to a Discardit II syringe by Becton Dickinson (Heidelberg, Germany) equipped with a polyethylene frit, in the following referred to as BD syringe. After coupling, the excess building block was recovered by quenching and precipitation with water. Centrifugation and purification of the pallet by chromatography yielded an average of 2 of 5 utilized equivalents.

Automated SPPS was performed on a Liberty Blue CEM (Matthews, USA) microwave-assisted peptide synthesizer.

The AAs were coupled twice per AA using the modified CarbomaMAX coupling (5 eq. aa, 10 eq. DIC, 5 eq. OxymaPure, 0.5 eq. DIPEA in DMF, 1: 75 °C, 170 W, 15 s, 2: 90 °C, 30 W, 105 s) method.

Manual coupling was performed using a Discover microwave reaction cavity by CEM (Matthews, USA). The resin was placed in a BD syringe. Double coupling was achieved by treatment with the coupling cocktail (5 eq. aa, 5 eq. HATU, 4.5 eq, HOAt, 10 eq. DIPEA in DMF) and supported by microwave irradiation (70 °C, 25 W, 10 min). Between all steps, the resin was washed (5 x DMF).

To obtain an uncharged N-terminus the resin bound peptide was treated with the acylation cocktail (10 % Ac_2O, 5 % DIPEA in DMF) for 10 min at room temperature. The process was repeated twice. Afterwards, the resin was washed (5 x DMF).

On Resin Metathesis

Macrocyclization of the N-terminally protected or acylated peptides was performed on resin. After SPPS the resin was washed successively with DMF (5 x), MeOH (5 x), and DCM (5 x) and dried in a desiccator. The resin was placed in a BD syringe and the catalyst (0.25 mg/ mg of resin) was added. The syringe was immediately afterwards quenched with argon. Degassed DCE (0.04 mL/ mg resin) was added and the mixture was shaken at 50 °C for 2 h. The resin was filtered off and the process was repeated with fresh catalyst and solvent to complete the reaction. After filtration, the resin was thoroughly washed with DCE (10×).

Cleavage from Resin

After synthesis, the resin was filtered off, washed successively with DMF (5 x), MeOH (5 x) and DCM (10×), and dried in vacuo. Acidic cleavage from the resin was achieved by treatment with a mixture of a) trifluoroacetic acid (TFA)/triisopropylsilane/water (95 : 2.5 : 2.5, 4 mL, 2 h, cleavage). The resin was extracted with additional TFA (4 mL) and the combined extracts were concentrated to 2 mL under a flow of nitrogen. The crude peptide was then precipitated in cold diethyl ether (10 mL) and isolated by centrifugation and decantation of the supernatant. The precipitate was washed twice with ice-cold diethyl ether and subsequently lyophilized.

Supplementary Information

Additional references cited within the Supporting Information[80–93]

Acknowledgements

This work was funded by Fonds der Chemischen Industrie and the Deutsche Forschungsgemeinschaft (DFG, German Research Foundation) under Germany's Excellence Strategy – EXC 2067/1 – 390729940. S. Bazzi thanks the Dorothea Schlözer Postdoctoral Programme of the Georg-August-Universität Göttingen for their support. Open Access funding enabled and organized by Projekt DEAL.

Conflict of Interests

The authors declare no conflict of interest.

Data Availability Statement

The data that support the findings of this study are available in the supplementary material of this article.

Keywords: Peptide Protein Interactions · Photocages · Photochemistry · Photopharmacology · Molecular Dynamics Simulations

[1] L. Wang, N. Wang, W. Zhang, X. Cheng, Z. Yan, G. Shao, X. Wang, R. Wang, C. Fu, *Sig. Transduct. Target Ther.* **2022**, *7*, 48.
[2] E. Daliri, D. Oh, B. Lee, *Food* **2017**, *6*, 32.
[3] M. Akbarian, A. Khani, S. Eghbalpour, V. N. Uversky, *IJMS* **2022**, *23*, 1445.

[4] R. Hartmann, J.-M. Wal, H. Bernard, A.-K. Pentzien, *CPD* **2007**, *13*, 897–920.
[5] S. La Manna, C. Di Natale, D. Florio, D. Marasco, *IJMS* **2018**, *19*, 2714.
[6] M. Pelay-Gimeno, A. Glas, O. Koch, T. N. Grossmann, *Angew. Chem. Int. Ed.* **2015**, *54*, 8896–8927.
[7] R. Månsson, H. Bysell, P. Hansson, A. Schmidtchen, M. Malmsten, *Biomacromolecules* **2011**, *12*, 419–424.
[8] A. Caporale, S. Adorinni, D. Lamba, M. Saviano, *Molecules* **2021**, *26*, 1219.
[9] R. L. Stanfield, I. A. Wilson, *Curr. Opin. Struct. Biol.* **1995**, *5*, 103–113.
[10] H. Wang, R. S. Dawber, P. Zhang, M. Walko, A. J. Wilson, X. Wang, *Chem. Sci.* **2021**, *12*, 5977–5993.
[11] L. D. Walensky, G. H. Bird, *J. Med. Chem.* **2014**, *57*, 6275–6288.
[12] L. Nevola, E. Giralt, *Chem. Commun.* **2015**, *51*, 3302–3315.
[13] P. Diderich, D. Bertoldo, P. Dessen, M. M. Khan, I. Pizzitola, W. Held, J. Huelsken, C. Heinis, *ACS Chem. Biol.* **2016**, *11*, 1422–1427.
[14] B. Li, H. Tang, A. Turlik, Z. Wan, X. Xue, L. Li, X. Yang, J. Li, G. He, K. N. Houk, G. Chen, *Angew. Chem. Int. Ed.* **2021**, *60*, 6646–6652.
[15] N. E. Shepherd, H. N. Hoang, G. Abbenante, D. P. Fairlie, *J. Am. Chem. Soc.* **2005**, *127*, 2974–2983.
[16] C. E. Schafmeister, J. Po, G. L. Verdine, *J. Am. Chem. Soc.* **2000**, *122*, 5891–5892.
[17] R. Rezaei Araghi, J. A. Ryan, A. Letai, A. E. Keating, *ACS Chem. Biol.* **2016**, *11*, 1238–1244.
[18] Y. Wu, Y.-H. Li, X. Li, Y. Zou, H.-L. Liao, L. Liu, Y.-G. Chen, D. Bierer, H.-G. Hu, *Chem. Sci.* **2017**, *8*, 7368–7373.
[19] J. Iegre, J. S. Gaynord, N. S. Robertson, H. F. Sore, M. Hyvönen, D. R. Spring, *Adv. Ther.* **2018**, *1*, 1800052.
[20] Á. Roxin, J. Chen, C. C. G. Scully, B. H. Rotstein, A. K. Yudin, G. Zheng, *Bioconjugate Chem.* **2012**, *23*, 1387–1395.
[21] Y. Wu, A. Kaur, E. Fowler, M. M. Wiedmann, R. Young, W. R. J. D. Galloway, L. Olsen, H. F. Sore, A. Chattopadhyay, T. T.-L. Kwan, W. Xu, S. J. Walsh, P. de Andrade, M. Janecek, S. Arumugam, L. S. Itzhaki, Y. H. Lau, D. R. Spring, *ACS Chem. Biol.* **2019**, *14*, 526–533.
[22] C. M. Grison, G. M. Burslem, J. A. Miles, L. K. A. Pilsl, D. J. Yeo, Z. Imani, S. L. Warriner, M. E. Webb, A. J. Wilson, *Chem. Sci.* **2017**, *8*, 5166–5171.
[23] S. Learte-Aymamí, C. Vidal, A. Gutiérrez-González, J. L. Mascareñas, *Angew. Chem. Int. Ed.* **2020**, *59*, 9149–9154.
[24] L. Nevola, A. Martín-Quirós, K. Eckelt, N. Camarero, S. Tosi, A. Llobet, E. Giralt, P. Gorostiza, *Angew. Chem. Int. Ed.* **2013**, *52*, 7704–7708.
[25] R. Göstl, A. Senf, S. Hecht, *Chem. Soc. Rev.* **2014**, *43*, 1982.
[26] W. A. Velema, W. Szymanski, B. L. Feringa, *J. Am. Chem. Soc.* **2014**, *136*, 2178–2191.
[27] H. E. Bonfield, T. Knauber, F. Lévesque, E. G. Moschetta, F. Susanne, L. J. Edwards, *Nat. Commun.* **2020**, *11*, 804.
[28] D. Laczi, M. D. Johnstone, C. L. Fleming, *Chem. Asian J.* **2022**, *17*, DOI 10.1002/asia.202200200.
[29] I. M. Welleman, M. W. H. Hoorens, B. L. Feringa, H. H. Boersma, W. Szymański, *Chem. Sci.* **2020**, *11*, 11672–11691.
[30] K. Hüll, J. Morstein, D. Trauner, *Chem. Rev.* **2018**, *118*, 10710–10747.
[31] M. J. Fuchter, *J. Med. Chem.* **2020**, *63*, 11436–11447.
[32] A. Deiters, S. Kossatz, O. Vázquez, *ChemPhotoChem* **2021**, *5*, 1031–1032.
[33] J. Ramos-Soriano, M. C. Galan, *JACS Au* **2021**, *1*, 1516–1526.
[34] A. S. Lubbe, W. Szymanski, B. L. Feringa, *Chem. Soc. Rev.* **2017**, *46*, 1052–1079.
[35] N. Klöcker, F. P. Weissenboeck, M. van Dülmen, P. Špaček, S. Hüwel, A. Rentmeister, *Nat. Chem.* **2022**, *14*, 905–913.
[36] A. Bollu, N. Klöcker, P. Špaček, F. P. Weissenboeck, S. Hüwel, A. Rentmeister, *Angew. Chem. Int. Ed.* **2023**, *62*, DOI 10.1002/anie.202209975.
[37] F. P. Weissenboeck, H. Schepers, A. Rentmeister, *Angew. Chem. Int. Ed.* **2023**, DOI 10.1002/anie.202301778.
[38] M. Bose, D. Groff, J. Xie, E. Brustad, P. G. Schultz, *J. Am. Chem. Soc.* **2006**, *128*, 388–389.
[39] N. S. A. Crone, N. van Hilten, A. van der Ham, H. J. Risselada, A. Kros, A. L. Boyle, *Bioconjugate Chem.* **2023**, *34*, 345–357.
[40] A. C. Kneuttinger, K. Straub, P. Bittner, N. A. Simeth, A. Bruckmann, F. Busch, C. Rajendran, E. Hupfeld, V. H. Wysocki, D. Horinek, B. König, R. Merkl, R. Sterner, *Cell Chem. Biol.* **2019**, *26*, 1501–1514.e9.
[41] B. P. Corbet, J. M. Schlüter, E. R. Cotroneo, S. Crespi, N. A. Simeth, *Eur. J. Org. Chem.* **2023**, *26*, DOI 10.1002/ejoc.202201140.
[42] L. Albert, O. Vázquez, *Chem. Commun.* **2019**, *55*, 10192–10213.
[43] A. Nomura, A. Okamoto, *Chem. Commun.* **2009**, 1906.
[44] T. Muraoka, H. Cui, S. I. Stupp, *J. Am. Chem. Soc.* **2008**, *130*, 2946–2947.
[45] L. Albert, J. Nagpal, W. Steinchen, L. Zhang, L. Werel, N. Djokovic, D. Ruzic, M. Hoffarth, J. Xu, J. Kaspareit, F. Abendroth, A. Royant, G. Bange, K. Nikolic, S. Ryu, Y. Dou, L.-O. Essen, O. Vázquez, *ACS Cent. Sci.* **2022**, *8*, 57–66.
[46] L. Albert, A. Peñalver, N. Djokovic, L. Werel, M. Hoffarth, D. Ruzic, J. Xu, L. Essen, K. Nikolic, Y. Dou, O. Vázquez, *ChemBioChem* **2019**, *20*, 1417–1429.
[47] A. A. Beharry, G. A. Woolley, *Chem. Soc. Rev.* **2011**, *40*, 4422.
[48] D. C. F. Monteiro, E. Amoah, C. Rogers, A. R. Pearson, *Acta Crystallogr. Sect. D* **2021**, *77*, 1218–1232.
[49] M. Bojtár, K. Németh, F. Domahidy, G. Knorr, A. Verkman, M. Kállay, P. Kele, *J. Am. Chem. Soc.* **2020**, *142*, 15164–15171.
[50] L. Josa-Culleré, A. Llebaria, *ChemPhotoChem* **2021**, *5*, 296–314.
[51] J. M. Silva, E. Silva, R. L. Reis, *J. Controlled Release* **2019**, *298*, 154–176.
[52] P. Wang, M. Mondal, Y. Wang, *Eur. J. Org. Chem.* **2009**, *2009*, 2055–2058.
[53] P. Wang, *J. Photochem. Photobiol. A* **2017**, *335*, 300–310.
[54] P. Wang, L. Zhou, X. Zhang, X. Liang, *Chem. Commun.* **2010**, *46*, 1514–1516.
[55] E. Sokolovskaya, L. Barner, S. Bräse, J. Lahann, *Macromol. Rapid Commun.* **2014**, *35*, 780–786.
[56] S. P. Brown, A. B. Smith, *J. Am. Chem. Soc.* **2015**, *137*, 4034–4037.
[57] A. Borges, C. Nguyen, M. Letendre, I. Onasenko, R. Kandler, N. K. Nguyen, J. Chen, T. Allakhverdova, E. Atkinson, B. DiChiara, C. Wang, N. Petler, H. Patel, D. Nanavati, S. Das, A. Nag, *ChemBioChem* **2023**, *24*, DOI 10.1002/cbic.202200590.
[58] Y. Wu, H. Chau, W. Thor, K. H. Y. Chan, X. Ma, W. Chan, N. J. Long, K. Wong, *Angew. Chem. Int. Ed.* **2021**, *60*, 20301–20307.
[59] R. J. Mart, R. K. Allemann, *Chem. Commun.* **2016**, *52*, 12262–12277.
[60] G. A. Woolley, *Acc. Chem. Res.* **2005**, *38*, 486–493.
[61] E. Cataldi, M. Raschig, M. Gutmann, P. T. Geppert, M. Ruopp, M. Schock, H. Gerwe, R. Bertermann, L. Meinel, M. Finze, A. Nowak-Król, M. Decker, T. Lühmann, *ChemBioChem* **2023**, *24*, DOI 10.1002/cbic.202200570.
[62] A. M. Ali, G. A. Woolley, *Org. Biomol. Chem.* **2013**, *11*, 5325.
[63] A. A. Beharry, O. Sadovski, G. A. Woolley, *Org. Biomol. Chem.* **2008**, *6*, 4323.
[64] J. Lee, H. Lee, C. Kim, *New J. Chem.* **2020**, *44*, 14777–14780.
[65] J. Deng, X. Wu, G. Guo, X. Zhao, Z. Yu, *Org. Biomol. Chem.* **2020**, *18*, 5602–5607.
[66] S. Samanta, G. A. Woolley, *ChemBioChem* **2011**, *12*, 1712–1723.
[67] L. Lorenz, U. Kusebauch, L. Moroder, J. Wachtveitl, *ChemPhysChem* **2016**, *17*, 1314–1320.
[68] V. Peddie, A. D. Abell, *J. Photochem. Photobiol. C* **2019**, *40*, 1–20.
[69] W. H. So, C. T. T. Wong, J. Xia, *Chin. Chem. Lett.* **2018**, *29*, 1058–1062.
[70] T. Weinrich, M. Gränz, C. Grünewald, T. F. Prisner, M. W. Göbel, *Eur. J. Org. Chem.* **2017**, *2017*, 491–496.
[71] C. Hamerla, C. Neumann, K. Falahati, J. von Cosel, L. J. G. W. van Wilderen, M. S. Niraghatam, D. Kern-Michler, N. Mielke, M. Reinfelds, A. Rodrigues-Correia, A. Heckel, J. Bredenbeck, I. Burghardt, *Phys. Chem. Chem. Phys.* **2020**, *22*, 13418–13430.
[72] J. R. Litowski, R. S. Hodges, *J. Biol. Chem.* **2002**, *277*, 37272–37279.
[73] B. Apostolovic, H.-A. Klok, *Biomacromolecules* **2008**, *9*, 3173–3180.
[74] D. Wang, K. Chen, G. Dimartino, P. S. Arora, *Org. Biomol. Chem.* **2006**, *4*, 4074–4081.
[75] M. Rabe, C. Aisenbrey, K. Pluhackova, V. de Wert, A. L. Boyle, D. F. Bruggeman, S. A. Kirsch, R. A. Böckmann, A. Kros, J. Raap, B. Bechinger, *Biophys. J.* **2016**, *111*, 2162–2175.
[76] W. Kabsch, C. Sander, *Biopolymers* **1983**, *22*, 2577–2637.
[77] Q. Wang, F. Wang, R. Li, P. Wang, R. Yuan, D. Liu, Y. Liu, Y. Luan, C. Wang, S. Dong, *Chem. Eur. J.* **2023**, DOI 10.1002/chem.202203624.
[78] A. M. Schulte, G. Alachouzos, W. Szymański, B. L. Feringa, *J. Am. Chem. Soc.* **2022**, *144*, 12421–12430.
[79] A. Micsonai, F. Wien, É. Bulyáki, J. Kun, É. Moussong, Y.-H. Lee, Y. Goto, M. Réfrégiers, J. Kardos, *Nucleic Acids Res.* **2018**, *46*, W315–W322.
[80] K. Stranius, K. Börjesson, *Sci. Rep.* **2017**, *7*, 41145.
[81] C. Tian, K. Kasavajhala, K. A. A. Belfon, L. Raguette, H. Huang, A. N. Migues, J. Bickel, Y. Wang, J. Pincay, Q. Wu, C. Simmerling, *J. Chem. Theory Comput.* **2020**, *16*, 528–552.
[82] A. D. Becke, *Phys. Rev. A* **1988**, *38*, 3098–3100.
[83] F. Weigend, R. Ahlrichs, *Phys. Chem. Chem. Phys.* **2005**, *7*, 3297.
[84] S. Grimme, J. Antony, S. Ehrlich, H. Krieg, *J. Chem. Phys.* **2010**, *132*, 154104.
[85] S. Grimme, *J. Chem. Theory Comput.* **2019**, *15*, 2847–2862.
[86] C. I. Bayly, P. Cieplak, W. Cornell, P. A. Kollman, *J. Phys. Chem.* **1993**, *97*, 10269–10280.

[87] S. Izadi, R. Anandakrishnan, A. V. Onufriev, *J. Phys. Chem. Lett.* **2014**, *5*, 3863–3871.
[88] J. Jumper, R. Evans, A. Pritzel, T. Green, M. Figurnov, O. Ronneberger, K. Tunyasuvunakool, R. Bates, A. Žídek, A. Potapenko, A. Bridgland, C. Meyer, S. A. A. Kohl, A. J. Ballard, A. Cowie, B. Romera-Paredes, S. Nikolov, R. Jain, J. Adler, T. Back, S. Petersen, D. Reiman, E. Clancy, M. Zielinski, M. Steinegger, M. Pacholska, T. Berghammer, S. Bodenstein, D. Silver, O. Vinyals, A. W. Senior, K. Kavukcuoglu, P. Kohli, D. Hassabis, *Nature* **2021**, *596*, 583–589.
[89] J.-P. Ryckaert, G. Ciccotti, H. J. C. Berendsen, *J. Comput. Phys.* **1977**, *23*, 327–341.
[90] R. Salomon-Ferrer, A. W. Götz, D. Poole, S. Le Grand, R. C. Walker, *J. Chem. Theory Comput.* **2013**, *9*, 3878–3888.
[91] T. Steinbrecher, J. Latzer, D. A. Case, *J. Chem. Theory Comput.* **2012**, *8*, 4405–4412.
[92] D. A. Case, K. Belfon, I. Y. Ben-Shalom, S. R. Brozell, D. S. Cerutti, T. E. Cheatham III, V. W. D.Cruzeiro, T. A. Darden, R. E. Duke, G. Giambasu, M. K. Gilson, H. Gohlke, A. W. Goetz, R. Harris, S. Izadi, S. A. Izmailov, K. Kasavajhala, A. Kovalenko, R. Krasny, T. Kurtzman, T. S. Lee, S. LeGrand, P. Li, C. Lin, J. Liu, T. Luchko, R. Luo, V. Man, K. M. Merz, Y. Miao, O. Mikhailovskii, G. Monard, H. Nguyen, A. Onufriev, F. Pan, S. Pantano, R. Qi, D. R. Roe, A. Roitberg, C. Sagui, S. Schott-Verdugo, J. Shen, C. L. Simmerling, N. R. Skrynnikov, J. Smith, J. Swails, R. C. Walker, J. Wang, L. Wilson, R. M. Wolf, X. Wu, Y. Xiong, Y. Xue, D. M. Yorkand, P. A.Kollman, AMBER2020, University of California, San Francisco, **2020**.
[93] Gaussian 16, Revision A.03, M. J. Frisch, G. W. Trucks, H. B. Schlegel, G. E. Scuseria, M. A. Robb, J. R. Cheeseman, G. Scalmani, V. Barone, G. A. Petersson, H. Nakatsuji, X. Li, M. Caricato, A. V. Marenich, J. Bloino, B. G. Janesko, R. Gomperts, B. Mennucci, H. P. Hratchian, J. V. Ortiz, A. F. Izmaylov, J. L. Sonnenberg, D. Williams-Young, F. Ding, F. Lipparini, F. Egidi, J. Goings, B. Peng, A. Petrone, T. Henderson, D. Ranasinghe, V. G. Zakrzewski, J. Gao, N. Rega, G. Zheng, W. Liang, M. Hada, M. Ehara, K. Toyota, R. Fukuda, J. Hasegawa, M. Ishida, T. Nakajima, Y. Honda, O. Kitao, H. Nakai, T. Vreven, K. Throssell, J. A. Montgomery, Jr., J. E. Peralta, F. Ogliaro, M. J. Bearpark, J. J. Heyd, E. N. Brothers, K. N. Kudin, V. N. Staroverov, T. A. Keith, R. Kobayashi, J. Normand, K. Raghavachari, A. P. Rendell, J. C. Burant, S. S. Iyengar, J. Tomasi, M. Cossi, J. M. Millam, M. Klene, C. Adamo, R. Cammi, J. W. Ochterski, R. L. Martin, K. Morokuma, O. Farkas, J. B. Foresman, and D. J. Fox, Gaussian, Inc., Wallingford CT, **2016**.

Manuscript received: April 3, 2023
Revised manuscript received: May 17, 2023
Accepted manuscript online: May 22, 2023
Version of record online: July 25, 2023